Boundary layer stagnation point flow of the Casson hybrid nanofluid over an unsteady stretching surface

Cite as: AIP Advances **11**, 015016 (2021); https://doi.org/10.1063/5.0036232
Submitted: 19 November 2020 • Accepted: 08 December 2020 • Published Online: 05 January 2021

Wajdi Alghamdi, Taza Gul, Mehranullah Nullah, et al.

Boundary layer stagnation point flow of the Casson hybrid nanofluid over an unsteady stretching surface

Cite as: AIP Advances 11, 015016 (2021); doi: 10.1063/5.0036232
Submitted: 19 November 2020 • Accepted: 8 December 2020 •
Published Online: 6 January 2021

Wajdi Alghamdi,[1] Taza Gul,[2,3,a)] Mehranullah Nullah,[2] Ali Rehman,[2] S. Nasir,[4] A. Saeed,[4] and E. Bonyah[5]

AFFILIATIONS

[1]Department of Information Technology, Faculty of Computing and Information Technology, King Abdulaziz University, Jeddah 80261, Saudi Arabia
[2]Department of Mathematics, City University of Science and Information Technology, Peshawar 25000, Pakistan
[3]Higher Education Department Khyber Pakhtunkhwa, Khyber Pakhtunkhwa 25000, Pakistan
[4]Department of Mathematics, Abdul Wali Khan University, Mardan 23200, Pakistan
[5]Department of Mathematics Education, Akenten Appiah-Menka University of Skills Training and Entrepreneurial Development, Kumasi 00233, Ghana

[a)]**Author to whom correspondence should be addressed:** ebbonya@gmail.com

ABSTRACT

This work examines the behavior of hybrid nanofluid flow toward a stagnation point on a stretching surface. Copper and aluminum are considered as the hybrid nanoparticles. The Casson (non-Newtonian) fluid model is considered for hybrid nanofluids applying magnetic effects perpendicular to the surface. The governing equations are reduced to the ordinary differential equations using similarity transformations. The resulting equations are programmed in the Mathematica software using the OHAM-BVPh 2.0 package. The most important results of this investigation are the effects of different physical parameters such as β, M, S, and Pr on the velocity profile, temperature profile, skin friction coefficient, and local Nusselt number. With the escalation of the magnitude of the Prandtl number Pr, the temperature profile slashes down, while with the variation of the Eckert number, the temperature field improves. The key outcomes specify that the hybrid Casson nanofluid has a larger thermal conductivity when equated with traditional fluids. Therefore, the hybrid fluid plays an important role in the enhancement of the heat phenomena. The ratification of our findings is also addressed via tables and attained noteworthy results.

I. INTRODUCTION

The development of heat transport via the nanofluid has involved several scientists due to a lot of uses in various sectors, such as distillation and separation of biomolecules, biosensors, atomic system cooling, manufacture of glass fiber, thermal storing, solar water boilers, the field of defense, MRI, thermal absorption process, drag delivery, and transportation (thermal management in vehicles and cooling of the engine). In 1995 at the ASME Winter Annual conference, Choi[1] was the former scientist who introduced the term nanofluid. As a consideration of thermal assets, it is a core issue with the traditional type of heat carrying fluids, such as oil, lubricants, ethylene glycol $(CH_2OH)_2$, and water (H_2O), and they lack larger heat transport features. Nanofluids have invented revolutionary modification in fluid dynamics to enhance the thermal conductivity of conventional fluids.

Several scientists have investigated the problems related to nanofluids in both experimental and theoretical points of view. However, for producing distinct nanoparticles, an investigator needs various ingredients to make them. Such nanoparticles contain ceramic oxide (CuO, Al_2O_3), metals (Au, Ag, Cu), Ferro particles $(COFe_2O_4, Fe_3O_4, Mn–ZnFe_2O_4)$, and carbon in various forms (diamonds, graphite, and carbon nanotubes). The classical model for nanofluids was first presented by Maxwell.[2] References 3 and 4

are some review articles on nanoliquids. Some additional literature studies about heat transport in nanofluids can also be found in detail.[5–9] While some sort of nanofluid named hybrid nanofluid is presented, which is supposed to possess superior thermos-physical characteristics and excellent rheological behavior with enriched heat transport features, hybrid nanofluids are the extension of nanoliquid, which contains two distinct nanoparticles scatters in the base fluid. Such a novel kind of heat transport fluid attracts the consideration of many scientists to study the issues of the practical world. Hybrid nanofluids have been widely used in various sectors of heat transport, such as micro-electric and generator cooling, reduction of drugs, cooling of the atomic system, refrigeration, and cooling of the transformer. The concept of hybrid nanofluids to more improve the progressive features of the ordinary nanofluid was introduced by Suresh.[10] Recently, few numerical studies were examined on hybrid nanoliquids as a new idea in the field of science and technology. Devi and Devi[11,12] scrutinized the problems of heat transfer and flow of hydro-magnetic hybrid nanofluids ($Cu + Al_2O_3 + H_2O$) over a stretching surface. Chamkha and Tayebi[13] intended numerically the problem of heat transfer of copper and aluminum oxide hybrid nanoliquids in an annulus. The thermos-physical characteristics of the hybrid nanoliquid of TiO_2–Cu/H_2O with the Lorentz force were examined by Ghadikolaei *et al.*[14] Similarly, Hayat *et al.*[15] illustrated the rotating problem of Ag–CuO/water hybrid nanoliquids. The aqueous Titania–copper hybrid nanofluid stagnation point flow toward stretching cylinder was studied by Yousefi *et al.*[16] Subhani and Nadeem[17] studied the behavior of hybrid nanoliquid (Cu–TiO_2/H_2O) over a stretching sheet. Various authors explored the impact of physical factors on the flow of hybrid nanofluids using several proposed thermos-physical models; for instance, Hayat *et al.*,[18] Jamshed and Aziz,[18] Rostami *et al.*,[19] Dinarvand,[20] Saba *et al.*,[21,22] and Tlili *et al.*[23] For more details, a complete analysis of the hybrid nanofluid is considered in the book of Das *et al.*[24] and also in the works of Babu *et al.*,[25] Ashorynejed and Shahriari,[26] Leong *et al.*,[27] and Abbas *et al.*[28–30] from different aspects.

The phenomena of non-Newtonian liquid have a substantial character in the innovation of renewable and sustainable energy process development of contemporary trends. The Casson model is an exceptional non-Newtonian liquid model that has performed shearing thinning characteristics and stress. From such exclusive features, the Casson fluid becomes an ideal rheological fluid model for human blood, as in the human body, the red blood cells form rouleaux that creates stress. Parmar *et al.*[31] and Bhattacharyya[32] have examined the Casson model in various mathematical models. Nadeem *et al.*[33] scrutinized the chemical reaction impact on the flow of the Casson nanoliquid. Ullah *et al.*[34] worked on nanofluid flow passing over a porous surface. The numerical results of nanofluid (Casson) flow in the presence of slip effect were scrutinized by Kamran *et al.*[35] Also, the radiation influence on the energy expression over Casson flow was examined by Archana *et al.*[36] Gireesha *et al.*[37] explored the Casson flow and examined the impact of radiation and chemical reaction. Other than that study, the succeeding recent articles can be referred to as the additional information associated with the Casson nanofluid flows; for example, the works of Souayeh *et al.*,[38] Ullah *et al.*,[39] and Aziz and Afify.[40]

The behavior of stagnation point flow may be viscous/inviscid, steady or unsteady, normal/oblique, 2D or 3D, and forward/opposite. This type of flow is commonly entertained by the liquid motion close to the stagnation region of a firm media in liquid. Stagnation flows are very important in the reduction of friction, to maintain nuclear reactor coolness, and several other hydrodynamic and other industrial activities. Heimenz[41] introduced the idea of stagnation flow. Homann[42] deliberated the axisymmetric 3D stagnation flow. Later, Weidman[43] improved the Homann work for non-symmetric stagnation flow. Hamid *et al.*[44] studied the wavelet method and effects of model factors on such a type of flow of the Williamson nanoliquid. Amirhossein *et al.*[45] investigated the time dependent three-dimensional flow of the non-Newtonian (Maxwell) nanoliquid over a stretching surface.

Motivated by the work cited earlier, it is clear that the unsteady boundary layer stagnation flow of the hybrid nanoliquid ($Cu + Al_2 + H_2O$) passing over a stretching surface has not been studied yet. The main objective of this work is to fill this gap in the literature. Therefore, the Casson fluid model is employed along with magneto-hydrodynamics (MHD). The series solution for both velocity and temperature profiles is calculated by using OHAM; it is an influential analytical technique and various scholars employed the OHAM-BVPh 2.0 technique for several flow problems.[46–54] This method has the tendency that one can find a suitable parameter range for the modeled problems.[50,54] The velocity and temperature profiles along with the drag force and the rate of heat transfer are studied graphs for the various values of flow factors. The resting portion of the present analysis is planned as follows: The mathematical model is developed in Sec. II. In Sec. III, the analytical results for the final model boundary layer expressions are described.

II. MATHEMATICAL FORMULATION

Assume an incompressible, electrically conducting, unsteady, 2D boundary layer stagnation point flow with the transfer of heat of the non-Newtonian–Casson hybrid nanofluid ($Cu + Al_2 + Water$) past a stretching surface. The mathematical model and all other assumptions are set as in Ref. 32. It is also supposed that the rheological expression of state for the incompressible flow of a Casson fluid can be written as[33,34]

$$I_{mn} = \begin{cases} \left(\mu_B + p_y/\sqrt{2\pi}\right)2e_{nm}, & \pi > \pi_c, \\ \left(\mu_B + p_y/\sqrt{2\pi}\right)2e_{nm}, & \pi < \pi_c, \end{cases} \tag{1}$$

where μ_B is the plastic dynamic viscosity of the non-Newtonian fluid, p_y is the yield stress of the fluid, π is the product of the component of the deformation rate by itself, such as $\pi = e_{nm}$, and π_c is the critical value of π based on the non-Newtonian model. Also, the unsteady parameter $S = \frac{\gamma}{b}$, the Casson parameter is $\beta = \mu_B\sqrt{2\pi_c}/p_y$, and the magnetic field $M = \frac{\sigma B_0^2}{\rho_{nf}}$, and under the above conditions, the boundary layer equations are selected as[32]

$$\frac{\partial u}{\partial x} + \frac{\partial v}{\partial y} = 0, \tag{2}$$

$$\frac{\partial u}{\partial t} + u\frac{\partial u}{\partial x} + v\frac{\partial u}{\partial y} = \frac{dU_s}{dt} + U_s\frac{dU_s}{dx} + \upsilon_{hnf}\left(1 + \frac{1}{\beta}\right)\frac{\partial^2 u}{\partial y^2} + \frac{\sigma_{hnf}B_0^2}{\rho_{hnf}}(U_s - u), \tag{3}$$

$$\frac{\partial T}{\partial t} + u\frac{\partial T}{\partial t} + v\frac{\partial T}{\partial t} = \left[\frac{k}{\rho c_p}\right]_{hnf} \frac{\partial^2 T}{\partial y^2}. \tag{4}$$

Here, T is the temperature, the thermal conductivity is denoted by k, the fluid density is denoted by ρ, and the specific heat is denoted by c_p. The velocity components are u and v, the distance along the sheet is denoted by x, the distance perpendicular to the sheet is denoted by $y, U_s = a'x/(1-\alpha t)$ with $a' > 0$ is the velocity of the stagnation point, and the kinematic viscosity of the fluid is denoted by ν.

The boundary conditions for velocity and temperature are[32]

$$\begin{gathered} v = 0, u = U_w \ as\, y = 0\,;\ u \to U_s \ as\, y \to \infty, \\ T = T_w \ at\, y = 0; T \to T_\infty \ as\, y \to \infty. \end{gathered} \tag{5}$$

$U_w = \frac{a''x}{(1-at)}$ is the stretching sheet velocity, where a'' is stretching constant. The temperature of the sheet is denoted by T_w, while T_∞ is the free stream temperature, which is assumed to be constant.

To simplify Eqs. (2)–(5), we define the following stream function:

$$u = \frac{\partial \psi'}{\partial y} \text{ and } v = -\frac{\partial \psi'}{\partial x}. \tag{6}$$

The similarity transformation is defined as[45]

$$\psi = \sqrt{\frac{a\nu_f}{1-\alpha t}} x f(\eta) \text{ and } \eta = y\sqrt{\frac{a}{\nu_f(1-\alpha t)}},\ \theta(\eta) = \frac{T - T_\infty}{T_W - T_\infty}. \tag{7}$$

Substituting Eqs. (6) and (7) and Table I, the above equations are reduced to the following state:

$$\left(1+\frac{1}{\beta}\right) f''' + (1-\phi_1)^{2.5}(1-\phi_2)^{2.5}\left[(1-\phi_2)\left(1-\phi_1+\phi_1\frac{\rho_{s_1}}{\rho_f}\right) + \phi_2\frac{\rho_{s_2}}{\rho_f}\right]\left(-f'^2 + f''f - S\left(f' + \frac{\eta}{2}f''\right)\right) + M\left(1-f'\right) = 0, \tag{8}$$

$$\frac{k_{hnf}}{k_{bf}}\theta'' - \left[\left(1-\phi_1+\phi_1\frac{(\rho Cp)_{s_1}}{(\rho Cp)_f}\right)(1-\phi_2) + \frac{(\rho Cp)_{s_2}}{(\rho Cp)_f}\phi_2\right] \times \Pr\left(\left(\theta' f\right) + \frac{S}{2}\left(\eta\theta'\right)\right) = 0, \tag{9}$$

.

$$\begin{gathered} f(\eta) = 0, f'(\eta) = \frac{c}{a} \ at\, \eta = 0\,, f'(\eta) \to 1 \text{ as } \eta \to 0, \\ \theta(\eta) = 1 \text{ at } \eta = 0; \theta(\eta) \to 0 \text{ as } \eta \to \infty, \end{gathered} \tag{10}$$

where $\frac{c}{a}$ is the velocity ratio parameter.

A. The skin friction and Nusselt number

In this analysis, the two key important quantities are presented as follows:

$$C_{nf} = \frac{\tau_\omega}{\frac{1}{2}\rho U_\omega^2} \quad \text{and} \quad Nu = \frac{q_\omega}{k(T_\omega - T_0)}x. \tag{11}$$

B. Method of solution

Equations (7) and (8) are set up by the OHAM (Optimal Homotopy Analysis Method).[46–57] The initial guesses for the velocity and temperature profiles have been selected as

$$f_0(\eta) = \left(\eta + \frac{c}{a}\right)\left(1 - e^{-\eta}\right),\ \ \theta_0 = e^{-\eta}. \tag{12}$$

The initial guesses are obtained from higher order linear terms in Eqs. (8) and (9) with the help of the initial and boundary conditions in Eq. (10),

$$L_f = f''',\ \ L_\theta = \theta''. \tag{13}$$

The general solutions obtained from Eq. (13) are as follows:

$$L_f\left(\mathbb{C}'_1 + \mathbb{C}'_2\eta + \mathbb{C}'_3\eta^2 + \mathbb{C}'_4\eta^3\right) = 0 \quad \text{and} \quad L_\theta\left(\mathbb{C}'_5 + \mathbb{C}'_6\eta\right) = 0. \tag{14}$$

Kamran *et al.*[35] presented this method to find the square residual error, so those of Eqs. (8) and (9) are collected as

$$\varepsilon_m^f = \frac{1}{n+1}\sum_{j=1}^{n}\left[\kappa_f\left(\sum_{j=1}^{n} f(\eta)_{\eta=j\delta\eta}\right)\right], \tag{15}$$

$$\varepsilon_m^\theta = \frac{1}{n+1}\sum_{j=1}^{n}\left[\kappa_\theta\left(\sum_{j=1}^{n} f(\eta)_{\eta=j\delta\eta}, \sum_{j=1}^{n}\theta(\eta)_{\eta=j\delta\eta}\right)\right]. \tag{16}$$

The entire square residual of the temperature and velocity profiles has been combined as[46–54]

$$\varepsilon_m^t = \varepsilon_m^f + \varepsilon_m^\theta. \tag{17}$$

III. RESULT AND DISCUSSION

The theme of this portion is to discuss the physical aspects of the above figures and tables and explain the real mechanism behind the flow and temperature variation due to the influential physical factors $\beta, M, S, \Pr$, and $\phi_1 = \phi_2$.

The effective thermo-physical behavior of copper and aluminum is mentioned in Table I. The numerical values of skin

TABLE I. The thermo-physical properties.

Nanofluid	Hybrid nanofluid
$\mu_{nf} = \frac{\mu_f}{(1-\phi)^{2.5}}$	$\mu_{hnf} = \frac{\mu_f}{(1-\phi_1)^{2.5}(1-\phi_2)^{2.5}}$
$\rho_{nf} = \phi\rho_s + (1-\phi)\rho_f$	$\rho_{hnf} = \{[(1-\phi_1)(1-\phi_2) + \phi_1 s_1]\} + \phi_2\rho_2$
$(\rho C_p)_{nf} = \phi(\rho C_p)_s + (1-\phi)(\rho C_p)_f$	$(\rho C_p)_{hnf} \doteq \left[\left\{(1-\phi_2)(1-\phi_1)(\rho C_p)_f\right\} + \phi_1(\rho C_p)_{s_1}\right] - \phi_2\rho(\rho C_p)_{s_2}$
$\frac{k_{nf}}{k_f} = \frac{k_s+(n-1)k_f-(n-1)\phi(k_f-k_s)}{k_s+(n-1)k_f+\phi(k_f-k_s)}$	$\frac{k_{hnf}}{k_{bf}} = \frac{k_{s_2}+(n-1)k_{bf}-(n-1)\phi_2(k_{bf}-k_{s_2})}{k_{s_2}+(n-1)k_{bf}+\phi_2(k_{bf}-k_{s_2})}$

TABLE II. Evaluation of the skin friction for the hybrid nanofluid when Pr = 11.6, $\phi = 0.5$, and $A = 0.7$.[10–12]

β	M	$f''(0)$ Cu + Casson	$f''(0)$ Cu + Al_2 + Casson
0.3	0.6	0.2297	0.1947
0.5		0.2316	0.2795
0.7	0.7	0.2414	0.3726
	0.8	0.2500	0.4699
	0.9	0.2645	0.6615

friction for the copper nanoliquid and Cu + Al_2 hybrid nanoliquid are presented in Table II. It is perceived that skin friction declines for higher values of M and β. Similarly, the mathematical values of the Nusselt number for both the nanofluid and hybrid nanofluid are presented in Table III. The Nusselt number decays for the growing credit of Pr. The heat transfer rate increases with the increase in the value of the nanoparticle volume fraction ϕ_1 and ϕ_2. The heat transfer rate is comparatively larger using the hybrid nanofluid Cu + Al_2. Also, the convergence of the OHAM-BVPh 2.0 package up to 25 orders of approximation is presented in Tables IV and V for both the nanofluid and hybrid nanofluid, respectively. Note that for the nanofluid (Cu + Casson) case, we consider ϕ_1, and for the hybrid nanofluid (Cu + Al_2) case, we consider ϕ_1 and ϕ_2, while for only Casson fluid, we assume $\phi_1 = 0 = \phi_2$. Figure 1 shows the geometry of the problem. Now, the behavior of these leading factors on the $f'(\eta)$ (velocity field) is deliberated in Figs. 2–5. The behavior of β on the $f'(\eta)$ (velocity) field for the Cu Casson nanofluid and Cu + Al_2 Casson hybrid nanofluid is displayed in Fig. 2. The $f'(\eta)$ profile in this figure decays with a rising estimation of β. The fact behind this conduct is that the rising estimation of β enhances the elasticity of hybrid nanofluids, which causes the hybrid nanofluid to become

TABLE III. Evaluation of the Nusselt number ($Re_x^{-1/2}Nu_x$) for hybrid nanofluids when $\beta = 0.9$ and $M = 5$.[10–12]

Pr	$\phi_1 = \phi_2$	$\theta'(0)$ Cu + Casson	$\theta'(0)$ Cu + Al_2 + Casson
10	0.01	0.8931	0.9907
15	0.01	0.5934	0.6823
20	0.01	0.2745	0.3739
10	0.02	1.1561	1.3564
10	0.03	1.3377	1.5489

TABLE IV. Convergence of the method for Cu + Al_2 + Water when Pr = 21, M = 1, $\phi_1 = \phi_1 = 0.01$.[10–12]

m	ε_m^f Cu + Al_2 + Water	ε_m^θ Cu + Al_2 + Water
5	$5.364\,38 \times 10^{-1}$	$2.867\,75 \times 10^{-1}$
10	$7.140\,94 \times 10^{-3}$	$1.487\,38 \times 10^{-2}$
15	$3.209\,443 \times 10^{-7}$	$1.072\,98 \times 10^{-4}$
20	$4.372\,98 \times 10^{-9}$	$8.541\,31 \times 10^{-5}$
25	$1.957\,87 \times 10^{-11}$	$7.944\,23 \times 10^{-6}$

TABLE V. Show the convergence of method for Cu + Water. When Pr = 21, M = 5, and $\beta = 0.1$.

m	ε_m^f Cu + Water	ε_m^θ Cu + Water
5	$1.079\,91 \times 10^{-1}$	$2.885\,74 \times 10^{-1}$
10	$5.652\,66 \times 10^{-2}$	$1.075\,9 \times 10^{-3}$
15	$4.123\,83 \times 10^{-3}$	$1.075\,9 \times 10^{-5}$
20	$3.461\,6 \times 10^{-4}$	$8.557\,21 \times 10^{-7}$
25	3.133×10^{-5}	$8.006\,632 \times 10^{-9}$

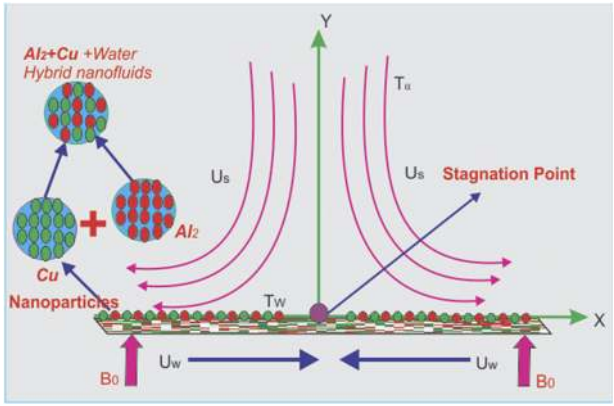

FIG. 1. Schematic of the studied geometry in the present analysis.

more viscous. Physically, in such a situation, the thickness of the momentum boundary layer reduces with the increase in β. Figure 3 disclosed the influence of (nanoparticle volume friction factors) ϕ_1 and ϕ_2 of the conventional Casson nanofluid and hybrid Casson nanofluid on $f'(\eta)$. Clearly, $f'(\eta)$ is declining against the growing value of ϕ_1 and ϕ_2. Physically, the higher values of ϕ_2 cause the thinning behavior of the momentum boundary layer. Thus, $f'(\eta)$ give a comparatively higher thickness of the boundary layer for the Cu + Al_2 Casson hybrid nanoliquid than the Cu Casson nano liquid. The impact of the M vs $f'(\eta)$ profile is captured in Fig. 4 for

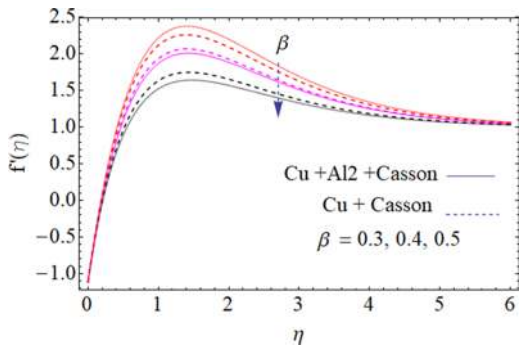

FIG. 2. Effect of the Casson parameter on the velocity profile.

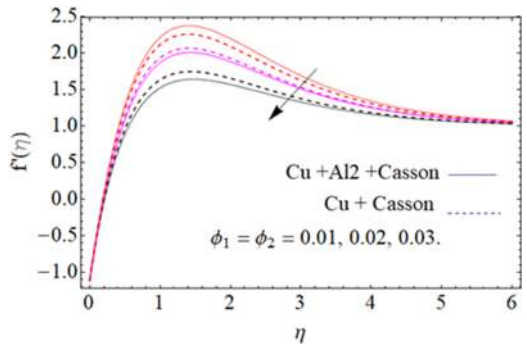

FIG. 3. Effect of the nanoparticle volume fraction on the velocity profile.

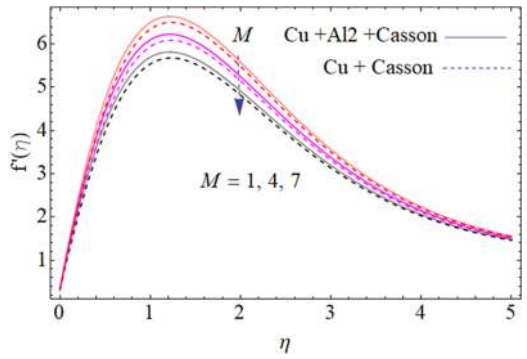

FIG. 4. Effect of magnetic field *M* on the velocity profile.

the Cu + Al_2 Casson hybrid nanoliquid and Cu Casson nanoliquid. Noticeably, this figure shows that improving the strength of *M*, the fluid flow reduced gradually for the nanoliquid as well as the hybrid nanoliquid. Such a state happens due to the production of a resistive Lorentz force. The opposing force enhances with the rising credit of *M*, which counteracts the motion of the fluid. This reducing trend in

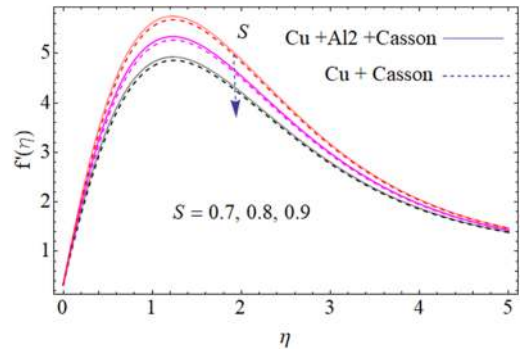

FIG. 5. Effect of unsteady parameter *S* on the velocity profile.

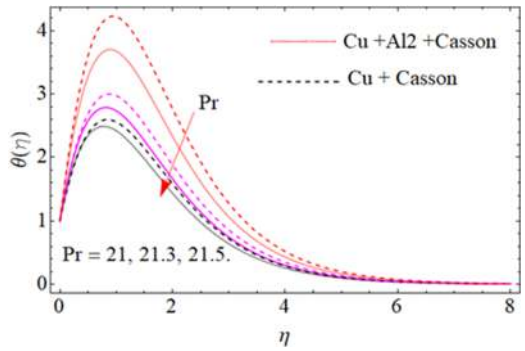

FIG. 6. Effect of the Prandtl number Pr vs temperature profile.

$f'(\eta)$ is perceived for both the Cu + Al_2 Casson hybrid nanoliquid and Cu Casson nanoliquid. The flow velocity behavior for various values of S is demonstrated in Fig. 5 for both the Cu + Al_2 Casson hybrid nanoliquid and Cu Casson nanoliquid. This figure expounds that $f'(\eta)$ at the surface is greater for a higher estimation of S. Therefore, the higher value of S augments the opposing force, causing a decline in the fluid velocity. To examine the trend of Pr on $\theta(\eta)$, Fig. 6 is schemed for both cases of the (Cu + Al_2 + Casson) Casson hybrid nanofluid and Cu Casson nanofluid. It is noticeable from the figure that $\theta(\eta)$ is a decreasing function of Pr. Therefore, it is justified due to the fact that thermal conductivity of the fluid is weaker with the escalated value of Pr and thus decreases the temperature of both the (Cu + Al_2) Casson hybrid nanofluid and Cu Casson nanofluid. The variation in *M* (magnetic parameter) on $\theta(\eta)$ profile is disclosed in Fig. 7 for both the Cu + Al_2 Casson hybrid nanoliquid and Cu Casson nanoliquid. Form the sketch, it is found that $\theta(\eta)$ is enhanced via the rising credit of *M*. The magnetic parameter and density of the hybrid nanofluid are inversely related to each other. Hence, intensification in *M* shrinks the fluid density, which causes temperature upsurges. The behavior of ϕ_1, ϕ_2 (nanoparticle volume friction) on $\theta(\eta)$ is drawn in Fig. 8. It is clear from the sketch that $\theta(\eta)$ is enhanced by increasing the values of ϕ_1 and ϕ_2. The rising effect is larger when the hybrid nanofluid is used.

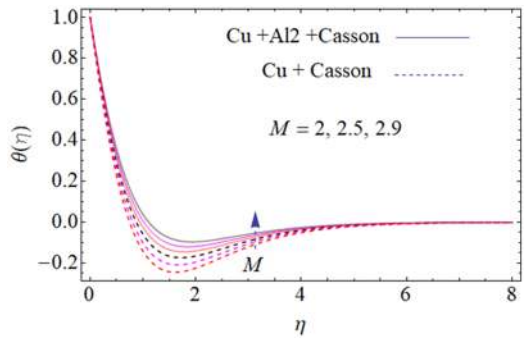

FIG. 7. Effect of the magnetic field *M* on the temperature profile.

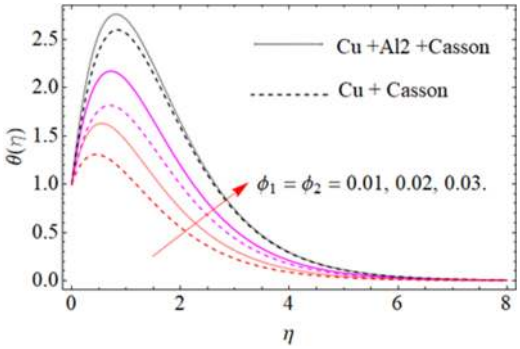

FIG. 8. Effect of the nanoparticle volume fraction on the temperature profile.

IV. CONCLUSION

In this paper, we explain the combination of copper Casson nanoliquid and copper–aluminum Casson hybrid nanoliquid. The nonlinear problem is modeled and solved by the analytical method (OHAM) to obtain analytic results, which analyzes the problem and the result of important parameters. The result of the important parameter is plotted and discussed for velocity and temperature. The effect of the hybrid nanoliquid is stronger than the simple nanoliquid in both velocity and temperature, and all the figures move parallel to the horizontal axis. The BVPh 2.0 package is used to obtain the converges of the problem up to 25 iterations. The findings of the present model are as follows:

- By improving the Casson parameter, the velocity field declines.
- By increasing the Prandtl number Pr, the temperature profile decreases.
- Increasing the magnetic field decreases the velocity field.
- Increasing ϕ_1 and ϕ_2 decreases the velocity field.
- Increasing ϕ_1 and ϕ_2 decreases the temperature field.

ACKNOWLEDGMENTS

The authors declare that they have no conflict of interest.

NOMENCLATURE

List of symbols

a''	stretching constant
B_0	magnetic field strength $\left(\mathrm{NmA}^{-1}\right)$
C_f	skin friction coefficient
$(C_p)_f$	specific heat of the base fluid (J/kgK)
f, g	dimensional velocity profiles
k_{nf}	thermal conductivity $(\mathrm{Wm}^{-1}\,\mathrm{K}^{-1})$
Nu	Nusselt number
Pr	Prandtl number
p_y	yield stress of the fluid
S	stretching parameter
T	fluid temperature (K)
T_w	surface temperature (K)
U_s	stagnation point velocity
U_w	stretching velocity
u, v, w	velocity components $\left(\mathrm{ms}^{-1}\right)$

Greek symbols

Θ	dimensional heat profiles
β	casson variable
η	similarity variable
μ_B	plastic dynamic viscosity (mPa)
μ_f	dynamic viscosity of the base fluid (mPa)
ρ_{nf}	nanofluid density $\left(\mathrm{Kgm}^{-3}\right)$
σ	electrical conductivity
ψ	stream function
ϕ_1	volume fraction of the nanoparticle
ϕ_2	volume fraction of the hybrid fluid

Subscripts

f	base fluid
hnf	hybrid nanofluid
nf	nanofluid
S	solid nanoparticles

Abbreviations

CNT	carbon nanotube
MHD	magneto-hydrodynamics
MWCNT	multi wall carbon nanotube
OHAM	optimal homotopy analysis method
SWCNT	single wall carbon nanotube

DATA AVAILABILITY

The data that support the findings of this study are available within the article.

REFERENCES

[1] S. U. S. Choi, "Enhancing thermal conductivity of fluids with nanoparticles," Off Sci. Tech. Inf. Tech. Rep. **231**, 99–105 (1995).
[2] R. L. Hamilton and O. K. Crosser, "Thermal conductivity of heterogeneous two component systems," I & EC Fund. **1**, 182–191 (1962).
[3] C. Pang, J. W. Lee, and Y. T. Kang, "Review on combined heat and mass transfer characteristics in nanofluids," Int. J. Therm. Sci. **87**, 49–67 (2015).
[4] J. Sarkar, P. Ghosh, and A. Adil, "A review on hybrid nanofluids: Recent research, development and applications," Renewable Sustainable Eng. Rev. **43**, 164–177 (2015).
[5] R. Ellahi, S. M. Sait, N. Shehzad, and Z.Ayaz, "A hybrid investigation on numerical and analytical solutions of electro-magnetohydrodynamics flow of nanofluid through porous media with entropy generation," Int. J. Numer. Methods Heat Fluid Flow **30**(2), 834–854 (2020).
[6] M. Hassan, M. Marin, R. Ellahi, and S. Z. Alamri, "Exploration of convective heat transfer and flow characteristics synthesis by Cu–Ag/water hybrid-nanofluids," Heat Transfer Res. **49**(18), 1837–1848 (2018).
[7] A. Shahid, H. Huang, M. M. Bhatti, L. Zhang, and R. Ellahi, "Numerical investigation on gyrotactic microorganisms in nanofluids through porous media past a stretched surface," Mathematics **8**(3), 380 (2020).
[8] S. Z. Alamri, A. A. Khan, M. Azeez, and R. Ellahi, "Effects of mass transfer on MHD second grade fluid towards stretching cylinder: A novel perspective of cattaneo–christov heat flux model," Phys. Lett. A **383**, 276–281 (2019).

[9]N. Abbas, M. Y. Malik, M. S. Alqarni, and S. Nadeem, "Study of three dimensional stagnation point flow of hybrid nanofluid over an isotropic slip surface," Physica A **554**, 124020 (2020).
[10]S. Suresh, K. P. Venkitaraj, P. Selvakumar, and M. Chandrasekar, "Effect of Al_2O_3Cu/water hybrid nanofluid in heat transfer," Exp. Therm. Fluid Sci. **38**, 54–60 (2012).
[11]S. P. A. Devi and S. S. U. Devi, "Numerical investigation of hydromagnetic hybrid Cu–Al_2O_3/water nanofluid flow over a permeable stretching sheet with suction," Int. J. Nonlinear Sci. Numer. Simul. **17**, 249–257 (2016).
[12]S. S. U. Devi and S. P. A. Devi, "Heat transfer enhancement of Cu–Al_2O_3/water hybrid nanofluid flow over a stretching sheet," J. Niger. Math. Soc. **36**, 419–433 (2017).
[13]T. Tayebi and A. J. Chamkha, "Free convection enhancement in an annulus between horizontal confocal elliptical cylinders using hybrid nanofluids," Numer. Heat Transfer, Part A **70**, 1141–1156 (2016).
[14]S. S. Ghadikolaei, M. Yassari, H. Sadeghi, and K. Hosseinzadeh, "Investigation on thermophysical properties of TiO_2–Cu–H_2O hybrid nanofluid transport dependent on shape factor in MHD stagnation point flow," Powder Tech. **322**, 428–438 (2017).
[15]T. Hayat, S. Nadeem, and A. U. Khan, "Rotating flow of Ag–CuO/H_2O hybrid nanofluid with radiation and partial slip boundary effects," Eur. Phys. J. E **41**, 60–75 (2018).
[16]M. Yousefi, S. Dinarvand, M. Eftekhari Yazdi, and I. Pop, "Stagnation-point flow of an aqueous titania-copper hybrid nanofluid toward a wavy cylinder," Int. J. Numer. Methods Heat Fluid Flow **28**, 1716–1735 (2018).
[17]M. Subhani and S. Nadeem, "Numerical analysis of micropolar hybrid nanofluid," Appl. Nanosci. **9**, 447–459 (2018).
[18]W. Jamshed and A. Aziz, "Cattaneo-Christov based study of TiO_2–CuO/EG Casson hybrid nanofluid flow over a stretching surface with entropy generation," Appl. Nano Sci. **8**, 685–698 (2018).
[19]M. N. Rostami, S. Dinarvand, and I. Pop, "Dual solutions for mixed convective stagnation-point flow of an aqueous silica–alumina hybrid nanofluid," Chin. J. Phys. **56**, 2465–2478 (2018).
[20]S. Dinarvand, "Nodal/saddle stagnation-point boundary layer flow of CuO–Ag/water hybrid nanofluid: A novel hybridity model," Micro. Technol. **25**, 2609–2623 (2019).
[21]F. Saba, N. Ahmed, U. Khan, A. Waheed, M. Rafiq, and S. T. Mohyud-Din, "Thermophysical analysis of water based ($CuAl_2O_3$) hybrid nanofluid in an asymmetric channel with dilating/squeezing walls considering different shapes of nanoparticles," Appl. Sci. **8**, 1540–1549 (2018).
[22]F. Saba, N. Ahmed, U. Khan, and S. T. Mohyud-Din, "A novel coupling of (CNT-Fe_3O_4/H_2O) hybrid nanofluid for improvements in heat transfer for flow in an asymmetric channel with dilating/squeezing walls," Int. J. Heat Mass Transfer **136**, 186–195 (2019).
[23]I. Tlili, M. M. Bhatti, S. M. Hamad, A. A. Barzinjy, and S. A. Sheikholeslami, "Macroscopic modeling for convection of Hybrid nanofluid with magnetic effects," Physica A **534**, 2–10 (2019).
[24]S. K. Das, S. U. S. Choi, W. Yu, and T. Pradeep, *Nanofluids: Science and Technology* (Wiley-Interscience, New Jersey, 2007).
[25]J. A. R. Babu, K. K. Kumar, and S. S. Rao, "State-of-art review on hybrid nanofluids," Renewable Sustainable Energy Rev. **77**, 551–565 (2017).
[26]H. R. Ashorynejad and A. Shahriari, "MHD natural convection of hybrid nanofluid in an open wavy cavity," Results Phys. **9**, 440–455 (2018).
[27]K. Y. Leong, K. Z. Ku Ahmad, H. C. Ong, M. J. Ghazali, and A. Baharum, "Synthesis and thermal conductivity characteristic of hybrid nanofluids—A review," Renewable Sustainable Energy Rev. **75**, 868–878 (2017).
[28]N. Abbas, M. Y. Malik, and S. Nadeem, "Stagnation flow of hybrid nanoparticles with MHD and slip effects," Heat Trans. Asian Res. **49**, 180–196 (2020).
[29]N. Abbas, M. Y. Malik, and S. Nadeem, "On extended version of Yamada–Ota and Xue models in micropolar fluid flow under the region of stagnation point," Physica A **542**, 123512 (2020).
[30]S. Nadeem, N. Abbas, and M. Y. Malik, "Inspection of hybrid based nanofluid flow over a curved surface," Comput. Methods Programs Biomed. **189**, 105193 (2020).
[31]L. Parmar, S. B. Kulshreshtha, and D. P. Singh, "Effects of stenosis on Casson flow of blood through arteries," Int. J. Adv. Comput. Math. Sci. **4**, 257–268 (2013).
[32]K. Bhattacharyya, "Boundary layer stagnation-point flow of Casson fluid and heat transfer towards a shrinking/stretching sheet," FHMT **4**, 023003 (2013).
[33]S. Nadeem, R. U. Haq, and N. S. Akbar, "MHD three-dimensional boundary layer flow of Casson nanofluid past a linearly stretching sheet with convective boundary condition," IEEE Trans. Nanotech. **13**(1), 109–115 (2014).
[34]I. Ullah, I. Khan, and S. Shafie, "MHD natural convection flow of Casson nanofluid over nonlinearly stretching sheet through porous medium with chemical reaction and thermal radiation," Nanoscale Res. Lett. **11**, 527–540 (2016).
[35]A. Kamran, S. Hussain, M. Sagheer, and N. Akmal, "A numerical study of magnetohydrodynamics flow in Casson nanofluid combined with Joule heating and slip boundary conditions," Results Phys. **7**, 3037–3048 (2017).
[36]M. Archana, B. J. Gireesha, B. C. Prasannakumara, and R. S. R. Gorla, "Influence of nonlinear thermal radiation on rotating flow of Casson nanofluid," Nonlinear Eng. **7**(2), 91–101 (2017).
[37]B. J. Gireesha, M. R. Krishnamurthy, B. C. Prasannakumara, and R. S. R. Gorla, "MHD flow and nonlinear radiative heat transfer of a Casson nanofluid past a nonlinearly stretching sheet in the presence of chemical reaction," Nanosci. Technol.: Int. J. **9**(3), 207–229 (2018).
[38]B. Souayeh, M. G. Reddy, P. Sreenivasulu, T. Poornima, M. Rahimi-Gorji, and I. M. Alarifi, "Comparative analysis on non-linear radiative heat transfer on MHD Casson nanofluid past a thin needle," J. Mol. Liq. **284**, 163–174 (2019).
[39]I. Ullah, K. S. Nisar, S. Shafie, I. Khan, M. Qasim, and A. Khan, "Unsteady free convection flow of casson nanofluid over a nonlinear stretching sheet," IEEE Access **7**, 93076–93087 (2019).
[40]A. M. Aziz and A. A. Afify, "Effect of Hall current on MHD slip flow of Casson nanofluid over a stretching sheet with zero nanoparticle mass flux," Thermophys. Aeromech. **26**, 429–443 (2019).
[41]K. Hiemenz, "Die Grenzschicht an einem in den gleichformigen Flussigkeitsstrom eingetauchten geraden Kreiszlynder," Dinglers J. **326**, 321–324 (1911).
[42]F. Homann, "Der Einfluß großer Zähigkeit bei der Strömung um den Zylinder und um die Kugel," ZAMM - J. Appl. Math. Mech. **16**, 153–164 (1936).
[43]P. D. Weidman and Y. P. Ma, "The competing effects of wall transpiration and stretching on Homann stagnation-point flow," Eur. J. Mech. B: Fluids **60**, 237–241 (2016).
[44]M. Hamid, M. Usman, R. U. Haq, Z. H. Khan, and W. Wang, "Wavelet analysis of stagnation point flow of non-Newtonian nanofluid," Appl. Math and Mech. **40**, 1211–1226 (2019).
[45]G. Amirhossein, D. Saeed, A. Armen, and A. S. Mikhail, "Unsteady general three-dimensional stagnation point flow of a maxwell/buongiorno non-Newtonian nanofluid," J. Nanofluids **8**, 1544–1559 (2019).
[46]S. Liao, "An optimal homotopy-analysis approach for strongly nonlinear differential equations," Commun. Nonlinear Sci. Numer. Simul. **15**, 2003–2016 (2010).
[47]*Advances in the Homotopy Analysis Method*, edited by S. J. Liao (World Scientific Press, Singapore, 2013).
[48]T. Hayat, F. Haider, T. Muhammad *et al.*, "Three-dimensional rotating flow of carbon nanotubes with Darcy-Forchheimer porous medium," PLoS One **12**, e0179576 (2017).
[49]T. Gul, W. Noman, M. Sohail, and M. A. Khan, "Impact of the Marangoni and thermal radiation convection on the graphene-oxide-water-based and ethylene-glycol-based nanofluids," Adv. Mech. Eng. **11**(6), 1–9 (2019).
[50]T. Gul, J. Rahman, M. Bilal, A. Saeed, W. Alghamdi, S. Mukhtar, H. Alrabaiah, and E. Bonyah, "Viscous dissipated hybrid nanoliquid flow with Darcy-Forchheimer and forced convection over a moving thin needle," AIP Adv. **10**, 105308 (2020).
[51]S. Nasir, Z. Shah, S. Islam, E. Bonyah, and T. Gul, "Darcy Forchheimer nanofluid thin film flow of SWCNTs and heat transfer analysis over an unsteady stretching sheet," AIP Adv. **9**, 015223 (2019).

[52]Z. Shah, E. Bonyah, S. Islam, and T. Gul, "Impact of thermal radiation on electrical MHD rotating flow of Carbon nanotubes over a stretching sheet," AIP Adv. **9**, 015115 (2019).
[53]T. Gul, I. Haleem, I. Ullah *et al.*, "The study of the entropy generation in a thin film flow with variable fluid properties past over a stretching sheet," Adv. Mech. Eng. **10**(11), 1–15 (2018).
[54]W. Khan, M. Idress, T. Gul, M. A. Khan, and E. Bonyah, "Three non-Newtonian fluids flow considering thin film over an unsteady stretching surface with variable fluid properties," Adv. Mech. Eng. **10**(10), 1–17 (2018).
[55]T. Gul, M. Bilal, M. Shuaib, S. Mukhtar, and P. Thounthong, "Thin film flow of the water-based carbon nanotubes hybrid nanofluid under the magnetic effects," Heat Transfer Asian Res. **49**, 3211 (2020).
[56]T. Gul, A. Khan, M. Bilal, N. A. Alreshidi, S. Mukhtar, Z. Shah, and P. Kumam, "Magnetic dipole impact on the hybrid nanofluid flow over an extending surface," Sci. Rep. **10**, 8474 (2020).
[57]A. Tassaddiq, S. Khan, M. Bilal, T. Gul, S. Mukhtar, Z. Shah, and E. Bonyah, "Heat and mass transfer together with hybrid nanofluid flow over a rotating disk," AIP Adv. **10**, 055317 (2020).